Biochemistry

pubs.acs.org/biochemistry Article

Discovery and Mechanism of Small Molecule Inhibitors Selective for the Chromatin-Binding Domains of Oncogenic UHRF1

Wallace H. Liu, Robert E. Miner III, Brittany N. Albaugh, Gene E. Ananiev, Scott A. Wildman, and John M. Denu*

Cite This: *Biochemistry* 2022, 61, 354−366 Read Online

ACCESS | Metrics & More | Article Recommendations | Supporting Information

ABSTRACT: Chromatin abnormalities are common hallmarks of cancer cells, which exhibit alterations in DNA methylation profiles that can silence tumor suppressor genes. These epigenetic patterns are partly established and maintained by UHRF1 (ubiquitin-like PHD and RING finger domain-containing protein 1), which senses existing methylation states through multiple reader domains, and reinforces the modifications through recruitment of DNA methyltransferases. Small molecule inhibitors of UHRF1 would be important tools to illuminate molecular functions, yet no compounds capable of blocking UHRF1-histone binding in the context of the full-length protein exist. Here, we report the discovery and mechanism of action of compounds that selectively inhibit the UHRF1-histone interaction with low micromolar potency. Biochemical analyses reveal that these molecules are the first inhibitors to target the PHD finger of UHRF1, specifically disrupting histone H3 arginine 2 interactions with the PHD finger. Importantly, this unique inhibition mechanism is sufficient to displace binding of full-length UHRF1 with histones in vitro and in cells. Together, our study provides insight into the critical role of the PHD finger in driving histone interactions, and demonstrates that targeting this domain through a specific binding pocket is a tractable strategy for UHRF1-histone inhibition.

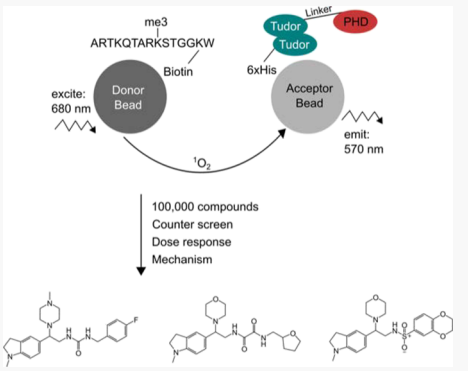

INTRODUCTION

Dysregulated chromatin structure and function are common phenomena during tumorigenesis, which is frequently driven by deleterious mutations of genes or improper gene expression.[1] These aberrant events are often caused by defects in the post-translational modification (PTM) patterns on the histone and DNA constituents of chromatin.[2,3] Therapeutic strategies targeting the molecular machinery that regulate PTM patterns—including the enzymes that install or remove the PTMs, as well as the "reader" domains that recognize the marks to enact signaling pathways—have proven success in the clinic. For example, established inhibitors of histone deacetylases (vorinostat) and DNA methyltransferases (5-azacytidine) demonstrate that the targeted enzymes drive cancer and can be effectively inhibited.[4−8]

Moreover, reader domains have emerged as promising targets in anticancer strategies. For instance, inhibitors of BET (bromodomain and extra terminal) bromodomains, which bind to specific acetylated lysines on histones and regulate oncogenic c-Myc expression, have progressed to clinical trials for leukemias.[9−13] Together, these breakthroughs highlight the idea of blocking protein−protein interactions through the surface areas within reader domain-histone interactions. Aside from bromodomains, however, strategies to modulate epigenetic pathways by blocking other reader domains represent not only untapped therapeutic potential, but also integral chemical biology tools to evaluate target function.[14] Here, we investigate the tractability and utility of small molecule inhibition of the TTD (tandem Tudor domain) and PHD finger (plant homeodomain) reader domains of UHRF1. UHRF1 utilizes multiple reader domains, including the linked TTD-PHD module and the SRA (SET and RING-associated) domain, to engage histone H3 trimethylated at lysine 9/unmodified at arginine 2 (H3K9me3/H3R2) and hemi-methylated DNA, respectively.[15−22] Under these conditions, UHRF1 recruits DNMT1 (DNA methyltransferase 1) to propagate DNA methylation, reinforcing a chromatin environment that silences tumor suppressor genes (TSGs).[16,17,23−26]

Overexpressed UHRF1 has been observed in numerous cancers, including those of colorectal, breast, lung, bladder, and liver origin.[27−31] In human cohorts, colon and liver cancer patients with high UHRF1 expression experience much lower survival rates and a higher probability of postsurgical recurrence.[25,30,32] Accordingly, RNAi-mediated knockdown of UHRF1 suppresses tumor growth in tissue culture experi-

Received: October 22, 2021
Revised: December 16, 2021
Published: February 10, 2022

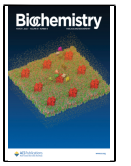

Downloaded via EASTERN MICHIGAN UNIV on July 11, 2022 at 17:08:27 (UTC).
See https://pubs.acs.org/sharingguidelines for options on how to legitimately share published articles.

ACS Publications © 2022 American Chemical Society

https://doi.org/10.1021/acs.biochem.1c00698
Biochemistry 2022, 61, 354−366

ments.[25,33] In HCT116, RKO, and SW620 colorectal cancer cells, all of which have high UHRF1 expression levels, UHRF1 knockdown reduces proliferation rates and/or invasiveness. Mice xenografted with HCT116 or RKO cells expressing wild-type UHRF1 readily develop tumors, while mice transplanted with UHRF1-deficient cells experience much less tumor burden and increased tumor latency.[25] Strikingly, a double mutation in the PHD finger that abolishes histone binding is sufficient to rescue this tumorigenic phenotype of UHRF1 in vivo.[25] Together, the data reveal that the UHRF1 chromatin-binding domains are necessary for UHRF1-dependent tumorigenicity.

Given these biological observations, we reason that small molecule inhibition of UHRF1 reader domains might constitute a valuable approach to understand the binding mechanisms that drive protein function. In addition, a small molecule inhibitor would be an important tool to determine the tractability of UHRF1 inhibition through blocking the histone-binding domains, a strategy that may potentially reverse aberrant methylation patterns in the cancer epigenome. Previous screening campaigns have uncovered TTD-histone small molecule inhibitors, which have the potential to become chemical probes for studying the functional consequences of H3K9me3 binding.[34−36] These molecules, however, do not appreciably inhibit the TTD-PHD module or the full-length protein, suggesting that the binding mechanisms driving the physiologically relevant UHRF1-histone interaction have not been successfully targeted. As a result, the tractability of inhibiting UHRF1-histone binding through small molecules is currently unclear. Here, we reveal novel small molecules identified from high-throughput screening (HTS) that exhibit low micromolar potency for displacement of the entire TTD-PHD module. Detailed biochemical analyses reveal that the molecules specifically target binding between the PHD finger of UHRF1 and the N-terminus of histone H3. We further demonstrate that the molecules exhibit in vitro and cellular activity in displacing full-length UHRF1 from histones. Together, our study not only reveals a critical determinant of histone binding driven by the PHD finger, but also provides important insight into the development of potent, selective, and cellularly active UHRF1 inhibitors.

MATERIALS AND METHODS

Preparation of Peptides and Proteins. H3K9me3 (ARTKQTAR{K-me3}STGGKW), H3K9me3$^{(Biotin)}$ (ARTKQTAR{K-me3}STGG{K-biotin}W), H3K9me3$^{(FAM)}$ (ARTKQTAR{K-me3}STGG{K-FAM}), H3K4me3 (ART-{K-me3}QTARKSTGGKW), and H3K4$^{(Biotin)}$ (ART{K-me3}-QTARKSTGG{K-biotin}W) peptides were purchased from Genscript at >95% purity. Unmodified H3$^{(FAM)}$ (ARTKQTARKSTGG{K-FAM}), H3K4me3$^{(FAM)}$ (ARTK{K-me3}QTARKSTGG{K-FAM}), and PBR$^{(FAM)}$ ({G-FAM}-KGKWKRKSAGGGPS) peptides were synthesized using solid-phase Fmoc-based synthesis on a Res Pep SL (InTavis) synthesizer, as previously described.[37] Biotinylated and FAM-labeled peptides were dissolved in water, while unlabeled peptides that were used as positive controls in screening experiments were dissolved in dimethyl sulfoxide (DMSO).

UHRF1$^{TTD-PHD}$ was inserted into a pET45b vector with an N-terminal 6xHis tag. The protein was expressed in BL21 (DE3) cells by induction with 0.5 mM IPTG at an optical density (OD) of 0.8 for 16 h at 18 °C. The bacterial pellet was resuspended on ice in 50 mM Tris, 350 mM NaCl, 20 mM imidazole, 1 mM βME, pH 7.5, along with protease inhibitors and DNase. The resuspension was sonicated at 20% amplitude with 1 s on/1 s off pulses for 10 min. The protein was clarified by centrifugation at 30, 000× *g* for 20 min at 4 °C, then loaded onto a 5 mL nickel-chelated column (HisTrap; GE Healthcare). The protein was eluted with an imidazole gradient up to 250 mM imidazole, then collected and dialyzed into 50 mM Tris, 50 mM NaCl, 1 mM DTT, 5% glycerol, pH 7.4 for loading onto a 5 mL Q column (GE Healthcare). The protein was eluted with a NaCl gradient up to 1.2 M NaCl. Finally, the protein was purified through a 120 mL HiLoad 16/600 Superdex 75 pg. column (GE Healthcare) in 20 mM HEPES, 150 mM NaCl, 1 mM DTT, pH 7.5.

Full-length UHRF1, incorporated in a pET28a vector bearing an N-terminal 6xHis tag, was expressed in BL21(DE3) pLysS cells by induction with 0.5 mM IPTG at an OD of 0.7 at 18 °C overnight. The cells were resuspended in 30 mM HEPES, 250 mM NaCl, 1 mM βME, 10 mM imidazole, pH 7.4, along with protease inhibitors and DNase. The resuspension was sonicated and clarified as described above, then loaded onto a 5 mL nickel-chelated column. The protein was eluted with an imidazole gradient up to 250 mM imidazole, then collected and dialyzed into 30 mM HEPES, 50 mM NaCl, 1 mM βME, pH 7.4. Because the protein had high relative 260 nm absorbance, the protein was loaded on a 5 mL heparin column (GE Healthcare) and eluted with a NaCl gradient up to 1.2 M NaCl. The resulting protein had no apparent nucleic acid contamination, as measured by absorbance at 260 nm.

GST-tagged proteins—including GST-UHRF1^{PHD}, GST-UHRF1$^{PHD;337A}$, GST-UHRF1$^{TTD-PHD;295A/296A}$, GST-AIRE^{PHD1}, GST-JARID1A^{PHD3}, GST-BHC80^{PHD}, and GST-RAG2^{PHD}—were expressed in BL21(DE3) cells by induction with 0.5 mM IPTG at an OD of 0.8 for 3 h at 25 °C. The cells were resuspended in wash buffer (50 mM Tris, 350 mM NaCl, 1 mM DTT, pH 7.4) along with protease inhibitors and DNase, then sonicated and clarified as described above. The resulting lysate was incubated with glutathione sepharose 4B resin (GE Healthcare) for 3 h, washed with wash buffer, and eluted in 50 mM Tris, 10 mM reduced glutathione, pH 7.4. The eluted protein was then extensively dialyzed in 20 mM HEPES, 150 mM NaCl, 1 mM DTT, pH 7.4.

AlphaScreen Experiments and HTS. For optimization of assay conditions, each of the UHRF1$^{TTD-PHD}$-H3K9me3$^{(Biotin)}$, KDM4A^{TTD}-H3K4me3$^{(Biotin)}$, KDM4C^{TTD}-H3K4me3$^{(Biotin)}$, and HP1^{CD}-H3K9me3$^{(Biotin)}$ interactions were tested in pilot AlphaScreen experiments with varying protein, peptide, and AlphaScreen bead concentrations.[37] The His-tagged methyl-lysine-binding domains were bound to Ni-NTA acceptor beads, while the biotinylated histone peptides were bound to streptavidin donor beads. Conditions that provided high *Z′*-factor scores and S/N ratios were used for subsequent screening efforts. Based on these criteria, 5 μg/mL each of donor and acceptor beads were selected, along with 50 nM UHRF1$^{TTD-PHD}$ and 50 nM H3K9me3$^{(Biotin)}$, 50 nM HP1^{CD} and 50 nM H3K9me3$^{(Biotin)}$, 40 nM KDM4A^{TTD} and 40 nM H3K4me3$^{(Biotin)}$, or 40 nM KDM4C^{TTD} and 40 nM H3K4me3$^{(Biotin)}$.

All HTS was conducted at the Small Molecule Screening Facility (UW-Madison). For HTS, compounds from the Life Chemicals diversity libraries were added to a final concentration of 33 μM in 1536-well plates (Perkin Elmer #6004290) using acoustic liquid handling (Labcyte Echo 550). Sixty-four

https://doi.org/10.1021/acs.biochem.1c00698
Biochemistry 2022, 61, 354−366

vehicle control wells (0.3% DMSO) and 64 positive control wells (50 μM H3K9me3) were also included. A master mix consisting of UHRF1$^{TTD\text{-}PHD}$, H3K9me3$^{(Biotin)}$, streptavidin donor, and Ni-NTA acceptor beads were incubated in StabilCoat immunoassay stabilizer buffer (Surmodics #SC01−2000) at room temperature. Five microliters of master mix was dispensed into each well using a Mantis liquid handler (Formulatrix). The plate was then allowed to incubate for 40 min with mild agitation. Luminescence was acquired on a PheraStar plate reader (BMG) with the following settings: 0.1 s settling time, 0.3 s excitation, and 0.6 s integration time with a 0.04 s delay between excitation and integration. Percentage inhibition was calculated by eq 1:

$$\text{Percentage inhibition} = 100 \times (1 - (X - A_{Min})/(A_{Max} - A_{Min})) \quad (1)$$

where X is the luminescence of the sample well, A_{Max} is the mean signal of the positive control wells in the same plate, and A_{Min} is the mean signal of the negative control wells.

After initial screening, compounds that displayed percentage inhibition values that were at least two standard deviations above the mean of the experimental plate were selected for retest. In addition, compounds known to interfere with the AlphaScreen signal from prior screening data (unpublished) were excluded from further experiments. In total, 870 compounds were rescreened using conditions identical to the initial HTS campaign. One hundred and ninety-one compounds that exhibited at least 25% inhibition were selected for counter screens under the conditions described above.

For dose response measurements, the AlphaScreen assay was conducted in the same manner, except compounds were added to wells at concentrations ranging from 0.78 to 100 μM. Dose response measurements were also repeated with freshly purchased compounds (Life Chemicals). IC_{50} was calculated by eq 2 from fitting in Prism 8 (GraphPad):

$$Y = \text{Min} + (\text{Max} - \text{Min})/(1 + 10\,\text{^}((\text{Log}IC_{50} - I) \times n)) \quad (2)$$

where Y is percentage inhibition at a given concentration (I) of the inhibitor, Min is the bottom of the curve, Max is the top of the curve, and n is the Hill slope (typically ~0.9 to 1.2).

Fluorescence Spectroscopy. Fifty compounds were tested in fluorescence polarization experiments as an orthogonal means to validate the observed compound-dependent UHRF1$^{TTD\text{-}PHD}$-H3K9me3 disruption in AlphaScreen experiments. The compounds included the 28 molecules deemed selective for UHRF1$^{TTD\text{-}PHD}$-H3K9me3 inhibition from counter screen results, as well as 22 other molecules that displayed >50% inhibition during the AlphaScreen retest. In the fluorescence polarization (FP) experiment, compounds were added to a final concentration of 35 μM in each 384-well plate (Thermo #262260), along with the same DMSO and vehicle controls used for AlphaScreens. A master mix consisting of 25 nM H3K9me3$^{(FAM)}$ and 2 μM UHRF1$^{TTD\text{-}PHD}$ was prepared in the StabilCoat immunoassay stabilizer buffer. Twenty microliters of master mix were dispensed into each well using a Mantis liquid handler. After 40 min incubation at room temperature, fluorescence was measured on a PheraStar plate reader with the following settings: excitation, 485 nm; emission, 520 nm; settling time of 0.2 s; and 200 flashes per well. Percentage inhibition was calculated by eq 1, except X is the fluorescence polarization of the sample well.

For dose response experiments with MLD3, MLD4, MLD5, and MLD13, compounds were purchased fresh from Life Chemicals at greater than 90% purity. All dose response FP experiments were conducted in 25 mM HEPES, 100 mM NaCl, 0.05% NP-40, pH 7.4 in a 384-well plate in 20 μL volumes. Twenty-five nM H3K9me3$^{(FAM)}$, H3K4me3$^{(FAM)}$, H3$^{(FAM)}$, or PBR$^{(FAM)}$ were bound to 1 μM UHRF1$^{TTD\text{-}PHD}$, 2 μM full-length UHRF1, 20 μM UHRF1^{TTD}, 1 μM GST-UHRF1$^{TTD\text{-}PHD;295A/296A}$, 1 μM GST-UHRF1^{PHD}, 15 μM GST-UHRF1$^{PHD;337A}$, 1 μM GST-AIRE^{PHD1}, 10 μM GST-BHC80^{PHD}, 0.5 μM GST-JARID1A^{PHD3}, or 5 μM GST-RAG2^{PHD}. The concentration of each protein was chosen to approximately align with the K_D of each respective interaction. Compounds were then added at the indicated concentrations, and fluorescence was read on a Synergy H4 plate reader (Biotek). Fluorescence anisotropy and percentage inhibition of FP experiments were calculated using eqs 3 and 4, respectively.

$$r = (I_{VV} - G \times I_{VH}) \times (I_{VV} + 2G \times I_{VH})\text{^} - 1 \quad (3)$$

where I_{VV} is the intensity of vertically polarized light emitting in the vertical plane, I_{VH} is the intensity of vertically polarized light emitting in the horizontal plane, and G is the grating factor ($G = I_{HV}/I_{HH}$) used to correct for instrument sensitivity to polarization bias.

$$\text{Percentage inhibition} = 100 \times (1 - (X - r_{Min})/(r_{Max} - r_{Min})) \quad (4)$$

where X is the anisotropy of the sample well, r_{Min} is the anisotropy of the FAM-labeled peptide fully bound to protein, and r_{Max} is the anisotropy of fully inhibited peptide-protein binding.

IC_{50} values were then calculated by eq 2, and K_D was calculated by a specific binding equation in Prism 8:

$$Y = \text{Bmax} \times X/(K_D + X) \quad (5)$$

where Bmax is the maximum binding, and X is the varying concentrations of protein added to the labeled peptide.

Tryptophan fluorescence experiments were conducted on a Quantamaster 4000 fluorometer (Horiba) using FelixGX software (v4.0). UHRF1^{PHD} (1 μM) was equilibrated in a 500 μL quartz cuvette (Starna) in 20 mM HEPES, 150 mM NaCl, 0.5% DMSO. Fifty microliters of the compound or 5 μM of the H3K9me3$^{(FAM)}$ peptide was then added. UHRF1^{PHD} was excited at 295 nm (slit width: 5 nm), and the emission was recorded from 315 to 400 nm (slit width: 15 nm). Under all conditions, the total absorbance at the excitation wavelength was <0.1. The change in tryptophan fluorescence was calculated by eq 6:

$$(\text{Fi} - F)/\text{Fi} \quad (6)$$

where Fi is the fluorescence signal of UHRF1^{PHD} alone at the fluorescence peak (330 nm), and F is the fluorescence signal of UHRF1^{PHD} when bound to the compound or the peptide.

Cell Culture and Bioluminescent Resonance Energy Transfer Experiments. LNCaP cells were maintained in RPMI 1640 (Life Technologies) supplemented with 10% FBS (Life Technologies). For bioluminescent resonance energy transfer (BRET) assays, pFC14K-HaloTag-H3, which appends a HaloTag to the C-terminus of histone H3, was purchased from Promega. Full-length UHRF1 was inserted into a

https://doi.org/10.1021/acs.biochem.1c00698
Biochemistry 2022, 61, 354−366

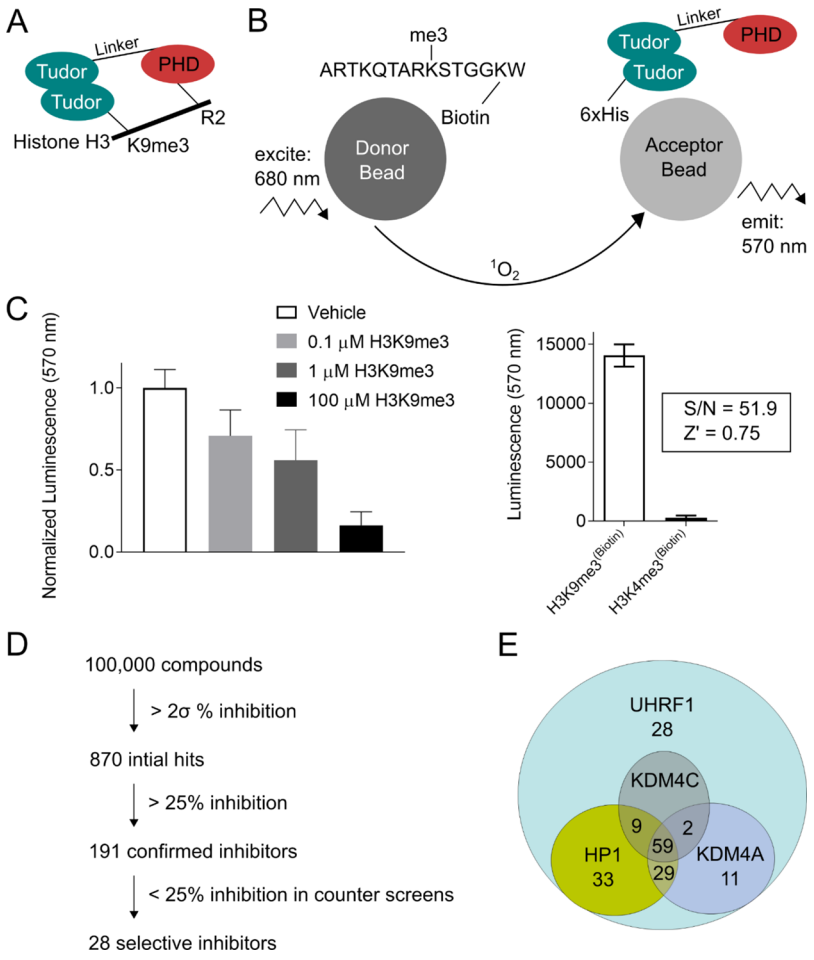

Figure 1. Screening strategies for the discovery of small molecule UHRF1$^{TTD\text{-}PHD}$-H3K9me3 inhibitors. (A) UHRF1 employs a linked TTD-PHD module to bivalently bind histone H3 at separate sites on the N-terminal histone peptide. (B) An AlphaScreen system was tailored to measure UHRF1$^{TTD\text{-}PHD}$-H3K9me3$^{(Biotin)}$ binding and displacement. In this setup, streptavidin-coated donor beads and nickel-chelated acceptor beads were bound with biotinylated H3K9me3 peptide and His-tagged UHRF1$^{TTD\text{-}PHD}$, respectively. When excited by 680 nm light, donor beads release singlet oxygen that excites chemicals present on proximal acceptor beads, which subsequently produce luminescence. (C) To demonstrate that the luminescence signal represents genuine UHRF1$^{TTD\text{-}PHD}$-H3K9me3$^{(Biotin)}$ binding, unlabeled H3K9me3 peptide was used to compete binding. Assay selectivity and robustness were determined by comparing the luminescence generated between the UHRF1$^{TTD\text{-}PHD}$-H3K9me3$^{(Biotin)}$ and UHRF1$^{TTD\text{-}PHD}$-H3K4me3$^{(Biotin)}$ interactions. Data are presented as mean ± s.d. from three independent experiments. (D) 100,000 compounds were screened using the AlphaScreen system in a 1536-well format. (E) After the retest, 191 confirmed hits were assayed in counter screens against KDM4A^{TTD}-H3K4me3$^{(Biotin)}$, KDM4C^{TTD}-H3K4me3$^{(Biotin)}$, and HP1^{CD}-H3K9me3$^{(Biotin)}$ interactions.

pFNnFK vector (Promega), which links an N-terminal NanoLuc enzyme to UHRF1. LNCaP cells were cotransfected with 1 μg of pFC14K-HaloTag-H3 and 10 ng of pFNnFK-NanoLuc-UHRF1 using lipofectamine 3000 (Thermo Fisher). After 16 h, the cells were replated in a 96-well plate (Costar 3917) at a density of 250,000 cells/mL and incubated with 618 Ligand (Promega) specific for HaloTag binding. The cells were then treated with 0.4% DMSO vehicle or 200 μM compound (0.4% DMSO). Eighteen hours after compound treatment, Nano-Glo substrate (Promega) was added to each well, and luminescence was recorded on a Synergy H4 plate reader (BioTek) using filters with 460 and 620 nm cut-off for Nanoluc and HaloTag-618 Ligand emission, respectively. The Milli BRET ratio was calculated by eq 7:

$$\text{milli BRET ratio} = (620\text{ nm luminescence}/460\text{ luminescence}) \times 1000 \quad (7)$$

For CellTiter-Glo analysis, 125 μL of the CellTiter-Glo reagent (Promega) was added to each well and allowed to shake for 5 min with mild agitation. After 30 min, luminescence was recorded.

For cellular lysis, LNCaP cells were lysed in 10 mM HEPES, 10 mM KCl, 0.05% NP-40, pH 7.4. For nuclear lysis, the extract was centrifuged at 18,000× *g* to resolve the nuclei and cytoplasm. The pelleted nuclei were then resuspended in 10 mM Tris, 0.2 mM $MgCl_2$, 1% Triton X-100, pH 7.4.

RESULTS

Identification of Selective UHRF1-H3 Inhibitors from an HTS Campaign. UHRF1 interacts with histone H3 through a multidomain module, which consists of the H3K9me3-binding TTD, a PHD finger that binds the H3 N-terminus, and a linker region in between that scaffolds the two domains together, supporting bivalent and synergistic H3 binding (Figure 1A).[38] This multivalent mode of binding suggests that the protein constructs used in screening strategies must be representative of the entire histone-binding module, to ensure full disruption of the physiologically relevant binding mechanism. Thus, we reasoned that screening for inhibitors of

https://doi.org/10.1021/acs.biochem.1c00698
Biochemistry 2022, 61, 354−366

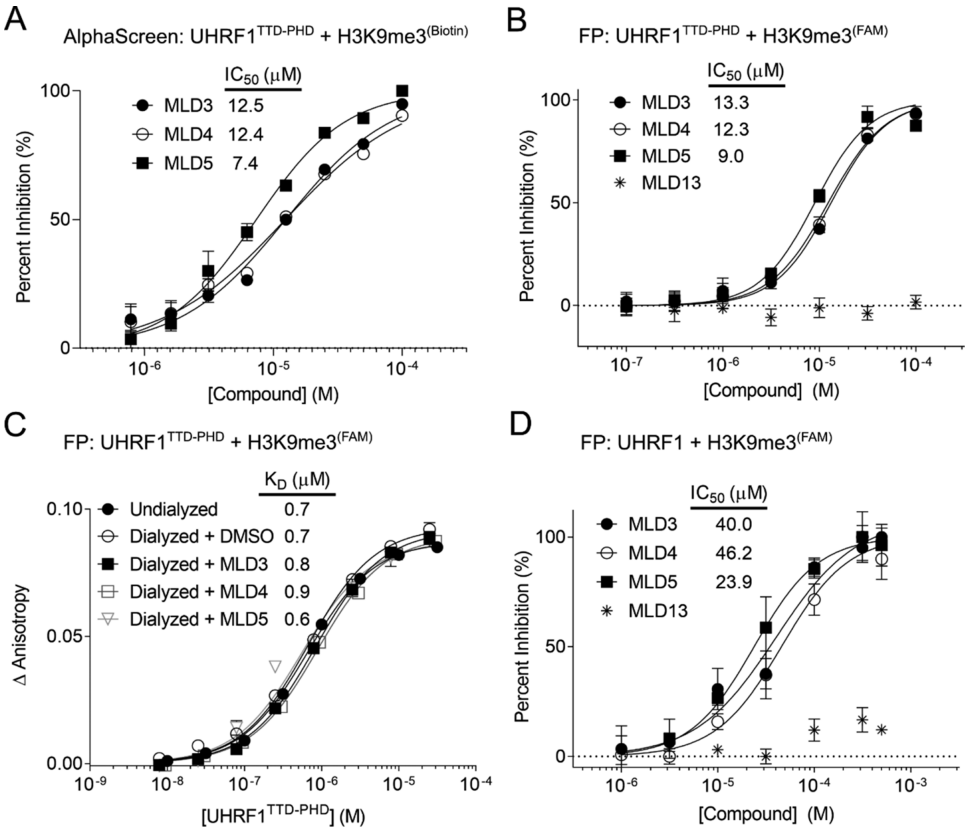

Figure 2. Identification of selective molecules with micromolar potency. (A) AlphaScreen dose response curves and half maximal inhibition constants for the three most potent and selective molecules. Data are presented as mean ± s.d. from three independent experiments. (B) IC_{50} values were also verified in the FP assay between $UHRF1^{TTD\text{-}PHD}$-$H3K9me3^{(FAM)}$. MLD13 was included as a negative control compound (Table 1). Data are presented as mean ± s.d. from three independent experiments. (C) To determine compound reversibility, compound or DMSO was allowed to dialyze with $UHRF1^{TTD\text{-}PHD}$ overnight before the $UHRF1^{TTD\text{-}PHD}$-$H3K9me3^{(FAM)}$ K_D was measured. The affinities were also compared to the K_D of $H3K9me3^{(FAM)}$ binding to undialyzed $UHRF1^{TTD\text{-}PHD}$. Data are presented as mean ± s.d. from three independent experiments. (D) In FP experiments, the potency of inhibition of MLD3−5 was determined for full-length UHRF1 binding to $H3K9me3^{(FAM)}$. Data are presented as mean ± s.d. from three independent experiments.

the intact TTD-PHD module among a diverse chemical library may yield insight into the mechanism of inhibition necessary for higher potency and selectivity.

To identify small molecule scaffolds capable of inhibiting the UHRF1-histone interaction, we developed an AlphaScreen assay for HTS. In this system, the TTD-PHD domains of His-tagged UHRF1 ($UHRF1^{TTD\text{-}PHD}$; residues 133−366) were tethered to Ni^{++}-chelated beads, which produced luminescence when excited by singlet oxygen generated from proximal donor beads bearing biotinylated H3K9me3 peptides ($H3K9me3^{(Biotin)}$) (Figure 1B). The luminescent signal was readily quenched by competition with an unlabeled H3K9me3 peptide and demonstrated high assay robustness ($Z' = 0.75$; Figure 1C). The AlphaScreen was further optimized in a 1536-well format, enabling screening in a miniaturized scale. Using this setup, we screened 100,000 compounds from the Life Chemicals diversity libraries at 33 μM concentration. Initial hits (870) were retested to confirm genuine inhibition in the AlphaScreen assay. In total, we identified 191 positive hits that exhibited >25% inhibition of $UHRF1^{TTD\text{-}PHD}$-$H3K9me3^{(Biotin)}$ binding (Figure 1D).

To determine the selectivity of our initial positive hits for $UHRF1^{TTD\text{-}PHD}$ against other epigenetic domains with similar binding properties, we designed counter screens for three other epigenetic protein−protein interactions. While $UHRF1^{TTD\text{-}PHD}$ is the only Tudor domain-containing module known to interact with H3K9me3, other Tudor domains display specificity for other methylated lysines at the H3 N-terminus.[39] In addition, the H3K9me3 modification is recognized by the chromodomain of HP1 ($HP1^{CD}$).[40] Accordingly, we developed AlphaScreen assays to detect binding and displacement of the $KDM4A^{TTD}$-$H3K4me3^{(Biotin)}$, $KDM4C^{TTD}$-$H3K4me3^{(Biotin)}$, and $HP1^{CD}$-$H3K9me3^{(Biotin)}$ interactions. For these counter screens, we tested the 191 initial hits from HTS (Figure 1D). We designated compounds as selective for $UHRF1^{TTD\text{-}PHD}$ if the compounds displayed less than 25% inhibition at 33 μM in each of the counter screens (Figure 1E). In total, 28 compounds exhibited selectivity for $UHRF1^{TTD\text{-}PHD}$, demonstrating that the chromatin-binding domains of UHRF1 can be selectively targeted by small molecules, even among other functionally similar interactions.

To independently validate hits in an orthogonal system, we developed an FP assay to monitor the $UHRF1^{TTD\text{-}PHD}$-H3K9me3 interaction (Figure S1). This method employs a H3K9me3 peptide C-terminally tagged with fluorescein (FAM; $H3K9me3^{(FAM)}$) and then complexed with $UHRF1^{TTD\text{-}PHD}$, permitting decreases in FAM polarization to report complex disruption. Along with the 28 selective hits (Figure 1E), we also tested additional compounds that exhibited >50% inhibition of $UHRF1^{TTD\text{-}PHD}$-H3K9me3 binding during initial screening conditions (Figure 1D; 50 compounds total). The results revealed that 15 compounds displayed greater than 50%

https://doi.org/10.1021/acs.biochem.1c00698
Biochemistry 2022, 61, 354−366

Table 1. AlphaScreen IC_{50} Values of Selected Compounds[a]

Manuscript ID / Pubchem CID	Chemical Structure	UHRF1$^{TTD-PHD}$- H3K9me3 (screening sample)	UHRF1$^{TTD-PHD}$- H3K9me3 (dry powder)	KDM4A^{TTD}- H3K4me3 (dry powder)	KDM4C^{TTD}- H3K4me3 (dry powder)	HP1^{CD}- H3K9me3 (dry powder)
MLD1 / 3153302	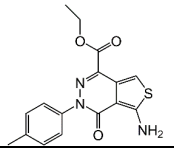	14	96.9	> 100	> 100	> 1000
MLD2 / 16837718	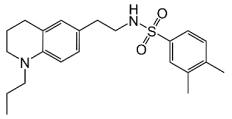	14.6	2.7	2.9	3.3	7.5
MLD3 / 44059703	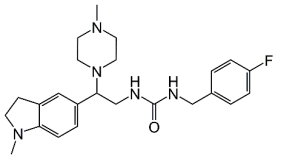	22.6	12.5	65.8	74	61.7
MLD4 / 44024750	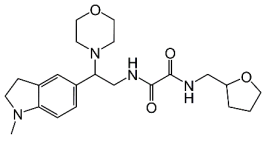	13.9	12.4	> 100	> 100	90.8
MLD5 / 16907713	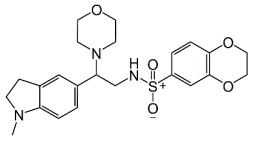	16.9	7.4	35.4	34.1	27
MLD6 / 16907733	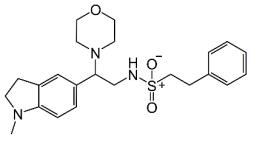	14.1	n.a.	n.d.	n.d.	n.d.
MLD7 / 7615918	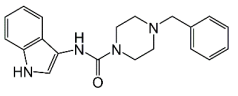	17.2	49.7	> 100	> 100	> 100
MLD8 / 42111134	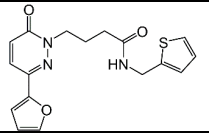	17.7	> 100	> 100	> 100	> 100
MLD9 / 6359866	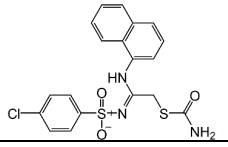	15.4	> 100	> 100	> 100	> 100
MLD10 / 5800155	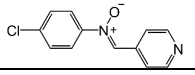	16.4	> 100	> 100	> 100	> 100
MLD13 / 44024897	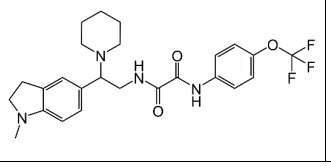	n.i.	n.i.	n.d.	n.d.	n.d.

[a]The potency values (μM) are colored as a heat map, where green colors represent greater compound potency and red colors represent weaker potency. n.i. no inhibition was detected. n.a. not available for purchase. n.d. not determined.

https://doi.org/10.1021/acs.biochem.1c00698
Biochemistry 2022, 61, 354−366

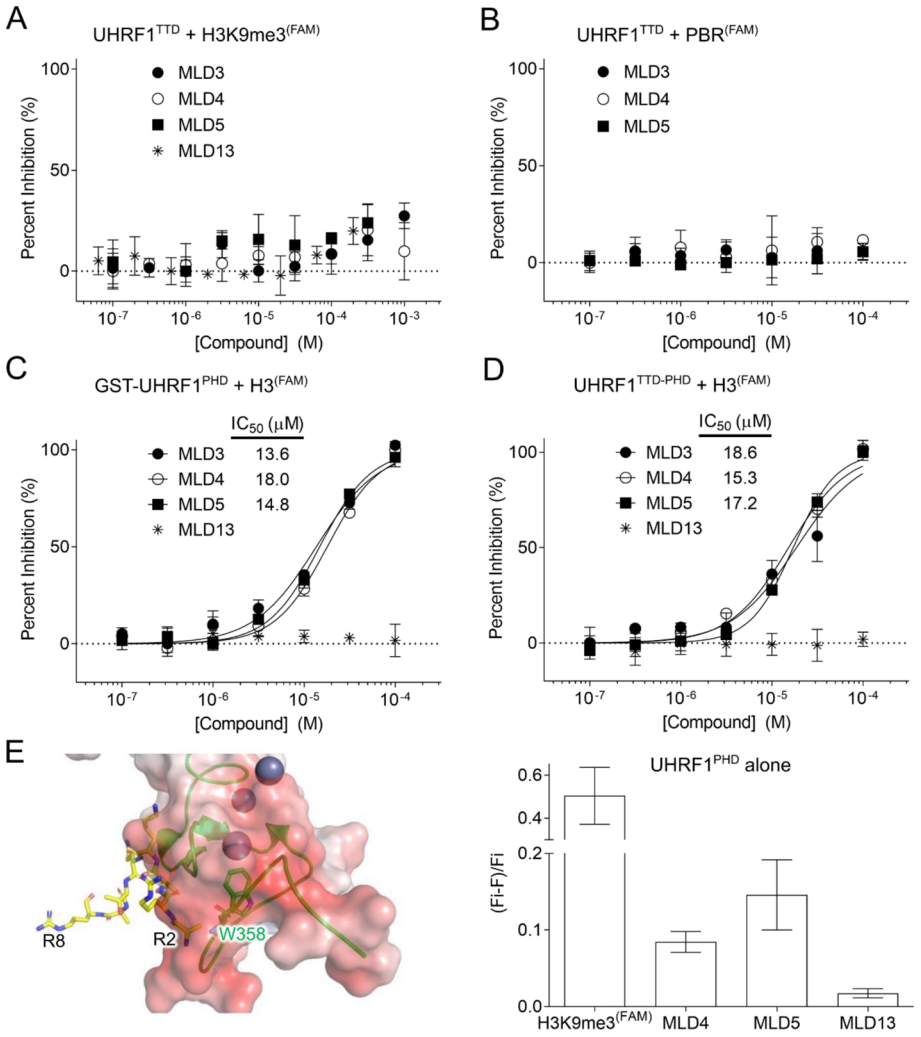

Figure 3. MLD3−5 specifically target the PHD finger of UHRF1. (A) FP analysis of UHRF1^{TTD}-H3K9me3$^{(FAM)}$ binding reveals that MLD3−5 do not inhibit the histone-binding capability of the UHRF1 TTD. Data are presented as mean ± s.d. from three independent experiments. (B) The compounds also did not inhibit binding between UHRF1^{TTD} and PBR$^{(FAM)}$, which binds to a TTD face different from the H3K9me3 peptide. Data are presented as mean ± s.d. from three independent experiments. (C) The compounds display specificity for inhibition of the GST-tagged PHD finger alone (residues 298−366) binding to unmodified H3$^{(FAM)}$, and fully inhibited (D) UHRF1$^{TTD-PHD}$ binding to unmodified H3$^{(FAM)}$. Data are presented as mean ± s.d. from three independent experiments. (E) W358 is the lone trytophan in UHRF1^{PHD} and resides near the histone-binding site (PDB: 3ZVY).[43,44] The fluorescence of UHRF1^{PHD} was readily quenched by 5 μM H3K9me3$^{(FAM)}$ peptide, which does not have a tryptophan. When incubated with 50 μM MLD4 or MLD5, UHRF1^{PHD} displayed greater W358 fluorescence quenching (14 and 8% quenching, respectively) than incubation with 50 μM MLD13 (<2% quenching). Data are presented as mean ± s.d. from three independent experiments.

inhibition at 35 μM, indicating that these compounds promote genuine UHRF1$^{TTD-PHD}$ displacement from histones and warranted more detailed characterization (Figure S1).

Determination of In Vitro Compound Potency. In prior reports of UHRF1 screening campaigns, compounds that block TTD-H3K9me3 binding have UHRF1$^{TTD-PHD}$-H3K9me3 inhibitory constants in the high micromolar (>100 μM) to millimolar regime.[34−36] To assess the potency of inhibition of our compounds, we tested the top 50 candidates in a dose response format using the AlphaScreen assay. Thirteen compounds promoted displacement of UHRF1$^{TTD-PHD}$-H3K9me3$^{(Biotin)}$ binding with IC_{50} values tighter than 20 μM (Figure S2A). Because the data were generated from compounds in long-term storage in DMSO, we selected 10 fresh compounds to purchase in dry powder form. The newer compounds were evaluated for potency in the UHRF1$^{TTD-PHD}$-H3K9me3$^{(Biotin)}$ interaction, as well as in the counter screens. Three compounds, MLD3−5, exhibited IC_{50} values between 7 and 12 μM, with at least fivefold selectivity over the interactions tested in counter screens (Figures 2A, S2B−D and Table 1). Notably, these molecules all share structurally similar scaffolds, characterized by either a sulfonamide or amide core attached to three-ringed groups: a methylindole, a morpholine or closely related methylpiperazine, and a variable ring (Table 1). Together, the compounds represent the only series of inhibitors to date that can block the TTD-PHD domains of UHRF1 in the low micromolar range.

To verify that the potency values observed in the bead-based AlphaScreen assay are representative of solution protein−peptide interactions, we also applied the FP assay to determine compound potency. In this more detailed follow-up experiment, the buffer was modified to include detergent (0.05% NP-40) to prevent nonspecific binding or aggregation effects from occurring. As a negative control, we also used a closely related compound, MLD13, which possessed similar ring functional groups to the other hits but displayed no inhibition of

https://doi.org/10.1021/acs.biochem.1c00698
Biochemistry 2022, 61, 354−366

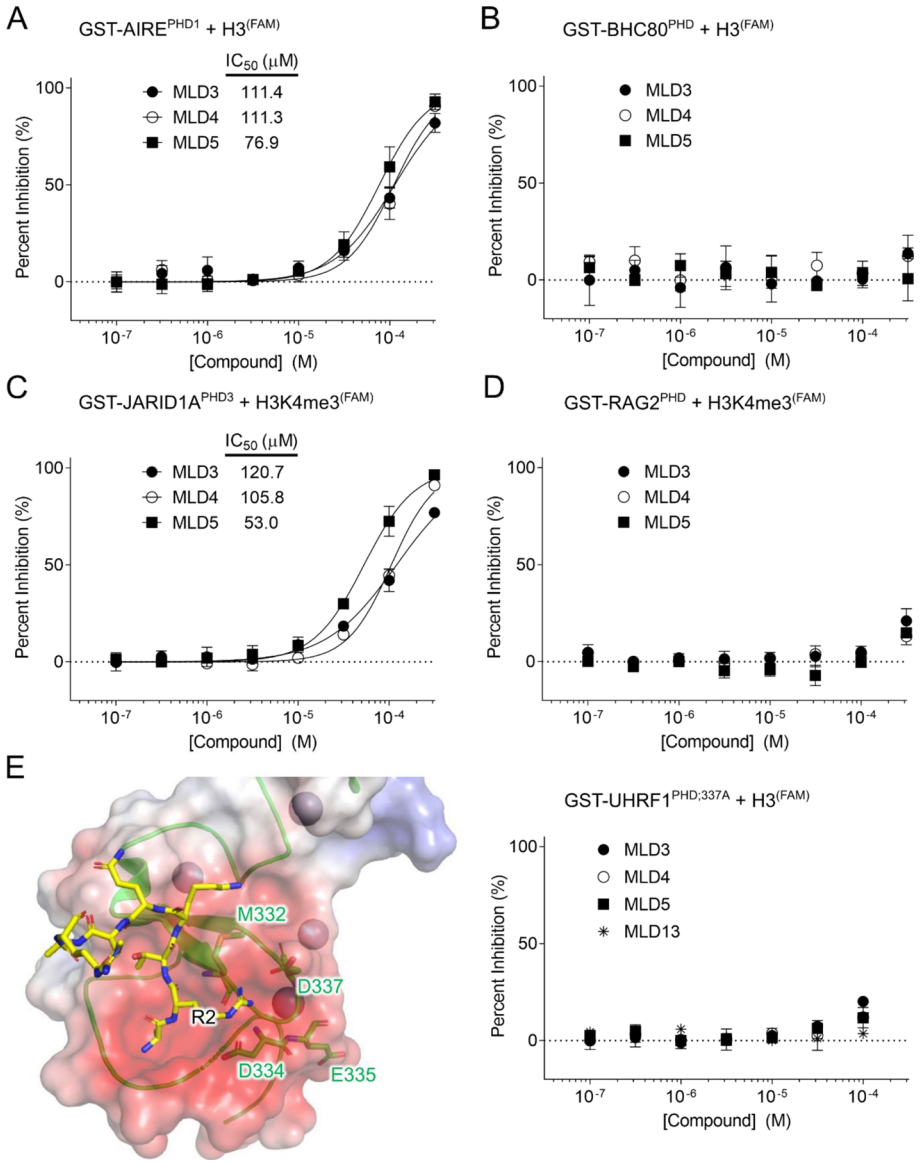

Figure 4. MLD3−5 are selective against other chromatin-binding PHD fingers. (A) The inhibitors display weak inhibition of GST-AIRE^{PHD1}-H3$^{(FAM)}$ binding by FP (IC_{50} ∼ 70−110 μM), but no inhibition of (B) GST-BHC80^{PHD}-H3$^{(FAM)}$ binding. Data are presented as mean ± s.d. from three independent experiments. (C) MLD3−5 also display weak inhibition for GST-JARID1A^{PHD3}-H3K4me3$^{(FAM)}$ (50−120 μM). Data are presented as mean ± s.d. from three independent experiments. (D) The compounds did not inhibit the GST-RAG2^{PHD}-H3K4me3$^{(FAM)}$ interaction. Data are presented as mean ± s.d. from three independent experiments. (E) Left panel: multiple residues within the H3R2 binding pocket in UHRF1^{PHD} contribute to the interaction with the histone peptide (PDB: 3ZVY).[43] In FP experiments, MLD3−5 did not inhibit UHRF1^{PHD}-H3$^{(FAM)}$ binding when PHD residue 337 was mutated from aspartate to alanine, suggesting that the inhibitors operate through a D337-dependent mechanism. Data are presented as mean ± s.d. from three independent experiments.

UHRF1$^{TTD-PHD}$-H3K9me3$^{(Biotin)}$ interactions (Table 1). In the FP assay, MLD3−5 inhibited the UHRF1$^{TTD-PHD}$-H3K9me3$^{(FAM)}$ interaction with similar IC_{50} values (9−13 μM) compared to the AlphaScreen format, while MLD13 did not inhibit the interaction (Figures 2B and S3A). The consistent results across multiple assay formats confirm that MLD3−5 inhibit UHRF1$^{TTD-PHD}$-H3K9me3 binding with micromolar potency and suggest that the conformation of UHRF1$^{TTD-PHD}$ capable of being inhibited on AlphaScreen beads is representative to that of UHRF1$^{TTD-PHD}$ in solution.

To assess the reversible binding of MLD3−5 to UHRF1$^{TTD-PHD}$, we prebound UHRF1$^{TTD-PHD}$ to each of the compounds individually and extensively dialyzed the complexes against buffer alone. After dialysis, we found that UHRF1$^{TTD-PHD}$ retained high binding affinity for H3K9me3$^{(FAM)}$ in FP assays, compared to untreated UHRF1$^{TTD-PHD}$ and UHRF1$^{TTD-PHD}$ dialyzed with the vehicle control (Figure 2C). Therefore, the MLD3−5 series of compounds demonstrates reversible inhibition of UHRF1$^{TTD-PHD}$-H3K9me3 binding.

Earlier efforts to identify UHRF1 TTD inhibitors have yielded compounds with moderate potency for the TTD, but significantly reduced potency on the histone-binding capability of the entire TTD-PHD module or the full-length protein.[34−36] To determine if the compounds inhibit H3K9me3 binding in the context of full-length UHRF1, we monitored displacement of UHRF1-H3K9me3$^{(FAM)}$ binding by FP. We found that MLD3−5 inhibited binding between H3K9me3$^{(FAM)}$ and

https://doi.org/10.1021/acs.biochem.1c00698
Biochemistry 2022, 61, 354−366

UHRF1 with IC_{50} values between 24 and 46 μM (Figure 2D). Thus, this class of compounds not only blocks the isolated histone-binding domains with micromolar potency, but also full-length UHRF1-histone binding.

MLD3−5 Inhibit the PHD Domain of UHRF1. Because MLD3−5 are the first identified compounds capable of blocking the histone-binding capability of full-length UHRF1, dissecting the inhibition mechanism of these compounds might provide insight into how the UHRF1-histone interaction can be more effectively blocked. To uncover which region of UHRF1—the TTD or the PHD—the compounds directly inhibit, we measured compound potency in the FP assay between histones and various UHRF1 constructs. Importantly, MLD3−5 did not inhibit interactions between H3K9me3$^{(FAM)}$ and the TTD construct alone (UHRF1^{TTD}; residues 127−285), revealing that the compounds do not target the trimethyl-binding pocket of UHRF1 (Figure 3A). In addition to binding the trimethyl group of H3K9me3, the TTD can also form intramolecular interactions with the linker region, as well as with the PBR (polybasic region) from the UHRF1 C-terminus.[35,38,41,42] Both of these intramolecular interactions utilize the same face of the TTD, although the PBR binds much tighter than the linker to the TTD.[42] Thus, we developed an FP assay with FAM-labeled PBR peptide (PBR$^{(FAM)}$; residues 643−657) bound in trans to UHRF1^{TTD}, in order to represent PBR and linker binding to the TTD, as well as to determine potential inhibition of TTD intramolecular interactions (Figure S3B). No inhibition of PBR$^{(FAM)}$-UHRF1^{TTD} was detected with addition of MLD3−5, revealing that our compounds do not target inter- or intramolecular binding interactions through the TTD (Figure 3B).

To determine if the compounds inhibit UHRF1^{PHD}-H3 binding, we utilized an FP assay to measure MLD3−5 potency when unmodified, FAM-labeled H3 peptide (H3$^{(FAM)}$) was bound to the PHD finger. An unmodified peptide was used because UHRF1^{PHD} binds specifically to the H3 N-terminus independent of the modification status of H3K9.[20,43,44] To obtain a high maximum polarization value, we included a GST-tag to the N-terminus of the PHD construct (GST-UHRF1^{PHD}; residues 298−366) (Figure S3C). The IC_{50} values reveal similar potency between inhibition of H3$^{(FAM)}$-GST-UHRF1^{PHD} with the H3K9me3$^{(FAM)}$-UHRF1$^{TTD-PHD}$ interaction (Figures 2A, B and 3C). In addition, binding between the unmodified histone peptide and UHRF1$^{TTD-PHD}$ was similarly inhibited by the compounds, further suggesting that MLD3−5 inhibit a contact point between the H3 N-terminus and the PHD finger (Figure 3D). Together, the results reveal that MLD3−5 specifically target the PHD finger of UHRF1, a unique mode of inhibition that is distinct from other known UHRF1-histone inhibitors that target the TTD.

The competitive inhibition of UHRF1-H3 by MLD3−5 suggests that the compounds might displace histone H3 through direct interactions with UHRF1^{PHD}. To confirm that the compounds directly bind with the domain, we monitored the intrinsic tryptophan fluorescence of UHRF1^{PHD} when the domain was incubated with compound. The PHD finger of UHRF1 possesses a lone tryptophan (W358), which is ∼8 Å from the H3R2 binding site and exhibits fluorescence capable of being quenched by histone peptide (Figures 3E and S4A).[44] We confirmed that addition of H3K9me3$^{(FAM)}$ peptide, which does not have a tryptophan, produced ∼50% quenching of W358 fluorescence (Figures 3E and S4B). Thus, if MLD3−5 also occupy a similar position in the domain, the compounds should also quench W358 fluorescence in the absence of histones. We found that incubation of UHRF1^{PHD} alone with MLD4 or MLD5 resulted in ∼8 and 14% quenching, respectively, while MLD13 did not appreciably change the fluorescence of W385 (<2%; Figures 3E and S4C−E). MLD3 has high intrinsic fluorescence that overlaps with tryptophan fluorescence and could not be used in this assay (Figure S4A). Together, the data suggest that direct binding between UHRF1^{PHD} and MLD4−5 causes an environmental change in the domain that leads to fluorescent quenching of W358.

MLD3−5 Are Selective for the PHD Domain of UHRF1 through the H3R2 Binding Pocket. Multiple PHD fingers are found in chromatin-binding proteins, with varying binding specificities for the N-terminus of histone H3.[45] To assess the selectivity of our inhibitors for the PHD of UHRF1 compared to other PHD fingers, we measured the potency of MLD3−5 in FP experiments on histone binding with GST-tagged constructs of AIRE^{PHD1}, JARID1A^{PHD3}, BHC80^{PHD}, and RAG2^{PHD} (Figure 4A−D). We observed no inhibition of BHC80^{PHD} and RAG2^{PHD} binding to histones by MLD3−5 (Figure 4B, D). Moreover, MLD3−5 exhibited 3−7× fold weaker potency for histone binding by the first PHD finger of AIRE and the third PHD finger of JARID1A (Figure 4A, C). Thus, MLD3−5 display greatest potency for UHRF1^{PHD} compared to other PHD fingers.

Notably, the PHD fingers of UHRF1, AIRE, and JARID1A that are inhibited by MLD3−5 all interact with arginine 2 on histone H3 (H3R2), while BHC80^{PHD} and RAG2^{PHD} do not contact this residue.[20,43,46−50] In UHRF1, the side chains of PHD residues D334 and D337 form ionic interactions with the guanidium group of H3R2 (Figure 4E).[20,43,50] Whereas mutation of D334 almost completely abrogates binding between UHRF1 and histone H3 in vitro, a D337A mutation weakens UHRF1^{PHD}-H3 binding by an order of magnitude.[20,43,51] Thus, to determine if the H3R2 binding pocket is involved in MLD3−5-dependent inhibition, we made a single point D337A mutation in GST-UHRF1^{PHD} (GST-UHRF1$^{PHD;337A}$), which impaired binding to histone H3 by ∼12-fold (Figure S3C). The formation of a bound complex, however, enabled competition experiments using these compounds. In FP experiments with the mutated construct bound to H3$^{(FAM)}$, MLD3−5 did not displace this interaction (Figure 4E). The result reveals that the compounds inhibit UHRF1-H3 binding specifically through a D337-dependent mechanism, which directly competes with histone binding.

MLD3−5 Displace Cellular UHRF1-Histone Binding. The selectivity and potency results suggest that MLD3, MLD4, and MLD5 may be suitable for further evaluation of compound effects in cell-based assays. To assess UHRF1-H3 binding in intact cells, we developed a NanoBRET assay, in which NanoLuc-tethered full-length UHRF1 and HaloTag-linked H3 were cotransfected into LNCaP cells.[52] LNCaP cells were chosen because of their low expression levels of endogenous UHRF1, which may otherwise interfere with compound effects.[53,54] When labeled with the fluorophore ligand, the HaloTag readily accepted luminescence from the NanoLuc enzyme (∼460 nm) and emitted distinct signal at ∼620 nm, providing a cellular BRET ratio that is exclusive to live cells (Figure S5A−C). Moreover, the BRET assay can be multiplexed with an adenosine triphosphate (ATP)-dependent luciferase after cell lysis (CellTiter-Glo) to assess cell viability.[55]

https://doi.org/10.1021/acs.biochem.1c00698
Biochemistry 2022, 61, 354−366

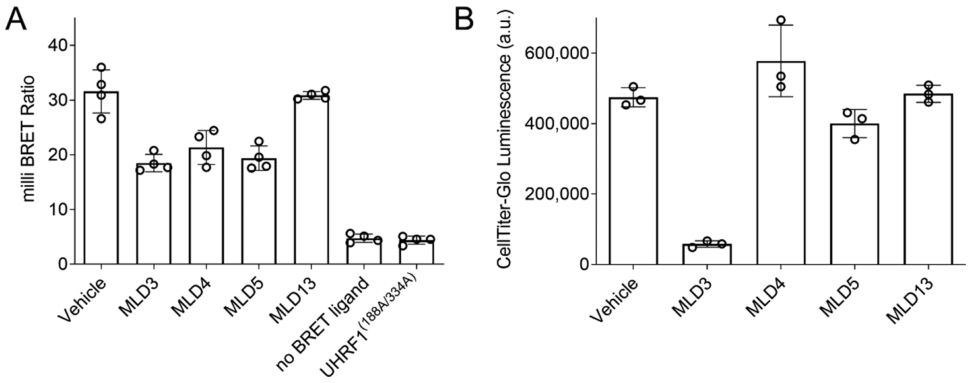

Figure 5. MLD3−5 displace UHRF1-histone H3 binding in cells. (A) The BRET ratio reports NanoLuc-UHRF1 and HaloTag-H3 binding in LNCaP cells. In the BRET assay, 200 μM MLD3−5 lowered the BRET ratio by ∼30 to 40%, compared to DMSO control and the MLD13 negative control compound. A control with no BRET ligand added, as well as a UHRF1 mutant defective in histone binding (UHRF1$^{188A/334A}$), are included. Milli BRET ratio was calculated as the acceptor luminescence normalized by donor luminescence, multiplied by 1000. Data are presented as mean ± s.d. from four independent experiments. (B) CellTiter-Glo measurements of extracellular ATP content in the same wells reveal that cell viability did not change with MLD4−5, but is decreased with MLD3. Data are presented as mean ± s.d. from three independent experiments.

To determine if MLD3−5 can displace UHRF1-H3 binding in cells, we cotransfected LNCaP cells with the NanoBRET plasmids and then added 200 μM MLD3−5, 200 μM of the negative control MLD13 compound, or equivalent percentage of DMSO to cells. Importantly, a 188A/334A double mutant known to be unable to bind histones exhibits a similar BRET ratio as a negative control (no BRET ligand added), demonstrating that the BRET effect observed is specific to UHRF1-H3 binding (Figure 5A). MLD3−5 induced a reduction in the BRET ratio between NanoLuc-UHRF1 and HaloTag-H3, indicating that these compounds were able to displace full-length UHRF1 from histones in live cells. MLD3−5 decreased the BRET ratio by ∼30−40%, compared to vehicle control and treatment with MLD13 (Figure 5A). The cells retained viability in the presence of MLD4 and MLD5, but viability with 200 μM MLD3 was markedly decreased (Figure 5B). In a dose response format, the compounds displayed dose-dependent displacement of NanoLuc-UHRF1 binding to HaloTag-H3, with noticeable decreases beginning at 100 μM compound concentration (Figure S6A−C). Together, the data indicate that MLD3−5 can actively disrupt UHRF1-H3 binding in intact cells at higher concentrations.

DISCUSSION

Chromatin, which consists of genomic DNA packaged into nucleosome units through interactions with histone proteins, serves as the template for most DNA-dependent processes. Alterations in chromatin structure and function underlie tumorigenic events that include oncogene activation and TSG suppression. Thus, pharmacological targeting of chromatin-modifying factors represents an emerging strategy to derepress TSGs or inactivate oncogenes. Despite interest in UHRF1 as a drug target, however, the current lack of potent histone-binding inhibitors suggests that this function of UHRF1 may not be pharmacologically tractable. Here, we reveal the mechanistic basis of effective UHRF1-histone inhibition by novel small molecules, which provide further biochemical insight into the function of the histone-binding module.

The small molecules uncovered in our screening campaign show that the TTD-PHD and full-length constructs of UHRF1 can be selectively inhibited through molecules that disrupt interactions between the PHD finger and histone H3. Inhibitors that targeted the TTD-H3K9me3 interaction specifically were not identified in the present screen. Previous screening efforts using TTD-only constructs found inhibitors with ∼30 μM potency, yet the same molecules poorly disrupted histone binding to TTD-PHD or full-length UHRF1.[34,36] Together, these results suggest that TTD-targeting inhibitors may not be effective on full-length UHRF1-H3 interactions, because the PHD finger drives histone interactions.

This observation may be due to a greater contribution by the PHD to binding energy in histone H3 interactions. In support of this idea, a Y188A mutation in the TTD methyllysine-binding pocket weakens binding to histones ∼2- to 10-fold in the context of the TTD-PHD module, yet D334A and D334A/E335A PHD mutations in TTD-PHD result in ∼30-fold and complete loss of binding, respectively.[51,56] In addition, we observed here that the PHD domain alone bound histone peptide with ∼5- to 6-fold greater affinity than the TTD alone (Figure S3A), consistent with another report.[42] Importantly, the TTD is dispensable for cancer cell methylation maintenance in cells and for UHRF1-dependent oncogenicity in vivo, while UHRF1 with a histone-binding deficient PHD mutant (D334A/E335A) is not oncogenic in mice.[25,57] Collectively, the data suggest a greater contribution to histone binding and oncogenicity by the PHD finger. As a result, screening with UHRF1 constructs that include the PHD finger is likely to be more representative of histone binding, and is more likely to uncover inhibitors that can contribute to mechanistic studies of the UHRF1 function in vitro and in cells.

Along these lines, this is the first chemical biology study to focus on inhibitors for the complete histone-binding module, revealing a series of compounds that inhibit full-length UHRF1-H3K9me3 binding with micromolar potency (Figure 2D). Biochemical follow-up experiments show that specific targeting of PHD-H3 binding is an inhibition mechanism that is sufficient to displace full-length UHRF1-H3 binding in vitro and in live cells (Figures 2D, 3C, D, and 5A). Significantly, relatively few reports of small molecules that specifically target PHD fingers exist, in contrast to myriad efforts to modulate the catalytic pockets or BET domains of epigenetic proteins.[58−60] The biochemical approaches here, however, not only show that the UHRF1^{PHD} finger is amenable to small molecule inhibition,

https://doi.org/10.1021/acs.biochem.1c00698
Biochemistry 2022, 61, 354−366

but also demonstrate that selective targeting of PHD fingers may be possible if the compounds exploit critical PHD-H3 binding differences. Specifically, MLD3−5 are not general PHD-H3 or PHD-H3K4me3 inhibitors, as shown by compound potency measurements with other PHD fingers (Figure 4A−D). Instead, the compounds appear to be selective for the H3R2 binding pocket in UHRF1. This pocket is especially critical for UHRF1-H3 interactions, as a D334A mutation dramatically curtails histone binding.[20,43] Here, we find that weakening this binding site through a D337A mutant nullifies MLD3−5-dependent inhibition, suggesting that the compounds directly compete interactions between the PHD finger and the H3 N-terminus (Figures 4E and S3C). As more efforts to discover UHRF1 inhibitors emerge, targeting this binding pocket would be a productive strategy to obtain inhibitors with more potent cellular activity.

In intact LNCaP cells, MLD3−5 promote decreases in UHRF1-histone binding at higher compound concentrations (Figure 5A). This cellular effect is in line with in vitro observations, as these PHD-targeting compounds inhibit full-length UHRF1-histone binding with micromolar potency (Figure 2D). We did not attempt compound concentrations greater than 200−400 μM, given that higher concentrations of compounds would lead to a greater likelihood of off-target effects. In line with this, MLD3 concentrations above 100 μM led to decreases in cell viability that are indicative of off-target effects (Figure 5B). The higher concentrations needed to observe an effect also suggest that greater potency or greater cell permeability is needed before the biological effects of TTD-PHD disruption from chromatin can be fully probed. The compounds identified in this study, however, reveal novel chemical structures that may be optimized into more potent molecules that are more suitable for future biological studies. Together, the results highlight the tractability of targeting the UHRF1 PHD finger to displace cellular UHRF1-histone binding, an important step toward the development of a potent chemical probe to study UHRF1 function.

■ ASSOCIATED CONTENT

Supporting Information

The Supporting Information is available free of charge at https://pubs.acs.org/doi/10.1021/acs.biochem.1c00698.

Additional data for orthogonal FP screening, dose response plots, K_D plots, fluorescence spectra, BRET assay development, and BRET dose response plots (PDF)

Accession Codes

UHRF1: UniProtKB Q96T88-1. Histone H3: UniProtKB P84243.

■ AUTHOR INFORMATION

Corresponding Author

John M. Denu − *Department of Biomolecular Chemistry, University of Wisconsin-Madison, Madison, Wisconsin 53706, United States; Wisconsin Institute for Discovery, University of Wisconsin-Madison, Madison, Wisconsin 53715, United States;* orcid.org/0000-0001-9415-0365; Phone: 608-316-4341; Email: john.denu@wisc.edu

Authors

Wallace H. Liu − *Department of Biomolecular Chemistry, University of Wisconsin-Madison, Madison, Wisconsin 53706, United States; Wisconsin Institute for Discovery, University of Wisconsin-Madison, Madison, Wisconsin 53715, United States*

Robert E. Miner III − *Department of Biomolecular Chemistry, University of Wisconsin-Madison, Madison, Wisconsin 53706, United States; Wisconsin Institute for Discovery, University of Wisconsin-Madison, Madison, Wisconsin 53715, United States*

Brittany N. Albaugh − *Department of Biomolecular Chemistry, University of Wisconsin-Madison, Madison, Wisconsin 53706, United States; Wisconsin Institute for Discovery, University of Wisconsin-Madison, Madison, Wisconsin 53715, United States*

Gene E. Ananiev − *Carbone Cancer Center, University of Wisconsin-Madison, Madison, Wisconsin 53706, United States*

Scott A. Wildman − *Carbone Cancer Center, University of Wisconsin-Madison, Madison, Wisconsin 53706, United States;* orcid.org/0000-0002-8598-0751

Complete contact information is available at: https://pubs.acs.org/10.1021/acs.biochem.1c00698

Funding

This work was supported by NIH grants F32 GM128399 and T32 DK007665 to W.H.L., GM059785 to J.M.D., and UW Institute for Clinical and Translational Research (UW-ICTR) grant AAD6475 to J.M.D.

Notes

The authors declare the following competing financial interest(s): J.M.D. is a consultant for Evrys Bio and the cofounder of Galilei BioSciences.

■ ACKNOWLEDGMENTS

The authors are grateful to Song Guo (UW-Madison) for technical assistance during the HTS campaign, Elise Wagner (UW-Madison) for providing the GST-tagged PHD plasmids, and Vyacheslav I. Kuznetsov (UW-Madison) for peptide synthesis support. The authors would also like to thank Marie Schwinn (Promega) and Danette Daniels (Promega) for providing technical assistance with the nanoBRET assay, Andrew Voter (UW-Madison) and Jim Keck (UW-Madison) for helpful discussions and use of the fluorometer, and Spencer Haws (UW-Madison) for assistance with cloning efforts.

■ REFERENCES

(1) Hanahan, D.; Weinberg, R. A. The Hallmarks of Cancer. *Cell* **2000**, *100*, 57−70.

(2) Baylin, S. B.; Jones, P. A. Epigenetic Determinants of Cancer. *Cold Spring Harbor Perspect. Biol.* **2016**, *8*, No. a019505.

(3) Shen, H.; Laird, P. W. Interplay between the Cancer Genome and Epigenome. *Cell* **2013**, *153*, 38−55.

(4) Kelly, W. K.; Connor, O. A. O.; Krug, L. M.; Chiao, J. H.; Heaney, M.; Curley, T.; MacGregore-Cortelli, B.; Tong, W.; Secrist, J. P.; Schwartz, L.; Richardson, S.; Chu, E.; Olgac, S.; Marks, P. A.; Scher, H.; Richon, V. M. Phase I Study of an Oral Histone Deacetylase Inhibitor , Suberoylanilide Hydroxamic Acid , in Patients With Advanced Cancer. *J. Clin. Oncol.* **2005**, *23*, 3923−3931.

(5) O'Connor, O. A.; Heaney, M. L.; Schwartz, L.; Richardson, S.; Willim, R.; MacGregor-Cortelli, B.; Curly, T.; Moskowitz, C.; Portlock, C.; Horwitz, S.; Zelenetz, A. D.; Frankel, S.; Richon, V.; Marks, P.; Kelly, W. K. Clinical Experience With Intravenous and Oral Formulations of the Novel Histone Deacetylase Inhibitor Suberoylanilide Hydroxamic Acid in Patients With Advanced Hematologic Malignancies. *J. Clin. Oncol.* **2006**, *24*, 166−173.

(6) Olsen, E. A.; Kim, Y. H.; Kuzel, T. M.; Pacheco, T. R.; Foss, F. M.; Parker, S.; Frankel, S. R.; Chen, C.; Ricker, J. L.; Arduino, J. M.; Duvic, M. Phase IIB Multicenter Trial of Vorinostat in Patients with Persistent, Progressive, or Treatment Refractory Cutaneous t-Cell Lymphoma. *J. Clin. Oncol.* **2007**, *25*, 3109−3115.
(7) Kantarjian, H.; Issa, J. J.; Rosenfeld, C. S.; Bennett, J. M.; Albitar, M.; Dipersio, J.; Klimek, V.; Slack, J.; de Castro, C.; Ravandi, F.; Helmer, R., III; Shen, L.; Nimer, S. D.; Leavitt, R.; Raza, A.; Saba, H. Decitabine Improves Patient Outcomes in Myelodysplastic Syndromes Results of a Phase III Randomized Study. *Cancer* **2006**, *106*, 1794−1803.
(8) Kantarjian, H. M.; Brien, S. O.; Cortes, J.; Giles, F. J.; Faderl, S.; Issa, J.-P.; Garcia-Manero, G.; Rios, M. B.; Shan, J.; Andreeff, M.; Keating, M.; Talpaz, M. Results of Decitabine (5-Aza-2′Deoxycytidine) Therapy in 130 Patients with Chronic Myelogenous Leukemia. *Cancer* **2003**, *98*, 522−528.
(9) Filippakopoulos, P.; Qi, J.; Picaud, S.; Shen, Y.; Smith, W. B.; Fedorov, O.; Morse, E. M.; Keates, T.; Hickman, T. T.; Felletar, I.; Philpott, M.; Munro, S.; McKeown, M. R.; Wang, Y.; Christie, A. L.; West, N.; Cameron, M. J.; Schwartz, B.; Heightman, T. D.; La Thangue, N.; French, C. A.; Wiest, O.; Kung, A. L.; Knapp, S.; Bradner, J. E. Selective Inhibition of BET Bromodomains. *Nature* **2010**, *468*, 1067−1073.
(10) Shi, J.; Vakoc, C. R. The Mechanisms behind the Therapeutic Activity of BET Bromodomain Inhibition. *Mol. Cell* **2014**, *54*, 728−736.
(11) Delmore, J. E.; Issa, G. C.; Lemieux, M. E.; Rahl, P. B.; Shi, J.; Jacobs, H. M.; Kastritis, E.; Gilpatrick, T.; Paranal, R. M.; Qi, J.; Chesi, M.; Schinzel, A. C.; McKeown, M. R.; Heffernan, T. P.; Vakoc, C. R.; Bergsagel, P. L.; Ghobrial, I. M.; Richardson, P. G.; Young, R. A.; Hahn, W. C.; Anderson, K. C.; Kung, A. L.; Bradner, J. E.; Mitsiades, C. S. BET Bromodomain Inhibition as a Therapeutic Strategy to Target C-Myc. *Cell* **2011**, *146*, 1−917.
(12) Mertz, J. A.; Conery, A. R.; Bryant, B. M.; Sandy, P.; Balasubramanian, S.; Mele, D. A.; Bergeron, L.; Sims, R. J., III Targeting MYC Dependence in Cancer by Inhibiting BET Bromodomains. *Proc. Natl. Acad. Sci. U. S. A.* **2011**, *108*, 16669−16674.
(13) Zuber, J.; Shi, J.; Wang, E.; Rappaport, A. R.; Herrmann, H.; Sison, E. A.; Magoon, D.; Qi, J.; Blatt, K.; Wunderlich, M.; Taylor, M. J.; Johns, C.; Chicas, A.; Mulloy, J. C.; Kogan, S. C.; Brown, P.; Valent, P.; Bradner, J. E.; Lowe, S. W.; Vakoc, C. R. RNAi Screen Identifies Brd 4 as a Therapeutic Target in Acute Myeloid Leukaemia. *Nature* **2011**, *478*, 524−528.
(14) James, L. I.; Frye, S. V. Chemical Probes for Methyl Lysine Reader Domains. *Curr. Opin. Chem. Biol.* **2016**, *33*, 135−141.
(15) Karagianni, P.; Amazit, L.; Qin, J.; Wong, J. ICBP90, a Novel Methyl K9 H3 Binding Protein Linking Protein Ubiquitination with Heterochromatin Formation. *Mol. Cell. Biol.* **2008**, *28*, 705−717.
(16) Bostick, M.; Kim, J. K.; Estève, P.-O.; Clark, A.; Pradhan, S.; Jacobsen, S. E. UHRF1 Plays a Role in Maintaining DNA Methylation in Mammalian Cells. *Science* **2007**, *317*, 1760−1765.
(17) Sharif, J.; Muto, M.; Takebayashi, S. I.; Suetake, I.; Iwamatsu, A.; Endo, T. A.; Shinga, J.; Mizutani-Koseki, Y.; Toyoda, T.; Okamura, K.; Tajima, S.; Mitsuya, K.; Okano, M.; Koseki, H. The SRA Protein Np95 Mediates Epigenetic Inheritance by Recruiting Dnmt 1 to Methylated DNA. *Nature* **2007**, *450*, 908−912.
(18) Arita, K.; Ariyoshi, M.; Tochio, H.; Nakamura, Y.; Shirakawa, M. Recognition of Hemi-Methylated DNA by the SRA Protein UHRF1 by a Base-Flipping Mechanism. *Nature* **2008**, *455*, 818−822.
(19) Avvakumov, G. V.; Walker, J. R.; Xue, S.; Li, Y.; Duan, S.; Bronner, C.; Arrowsmith, C. H.; Dhe-Paganon, S. Structural Basis for Recognition of Hemi-Methylated DNA by the SRA Domain of Human UHRF1. *Nature* **2008**, *455*, 822−825.
(20) Rajakumara, E.; Wang, Z.; Ma, H.; Hu, L.; Chen, H.; Lin, Y.; Guo, R.; Wu, F.; Li, H.; Lan, F.; Shi, Y. G.; Xu, Y.; Patel, D. J.; Shi, Y. PHD Finger Recognition of Unmodified Histone H3R2 Links UHRF1 to Regulation of Euchromatic Gene Expression. *Mol. Cell* **2011**, *43*, 275−284.
(21) Hashimoto, H.; Horton, J. R.; Zhang, X.; Bostick, M.; Jacobsen, S. E.; Cheng, X. The SRA Domain of UHRF1 Flips 5-Methylcytosine out of the DNA Helix. *Nature* **2008**, *455*, 826−830.
(22) Harrison, J. S.; Cornett, E. M.; Goldfarb, D.; DaRosa, P. A.; Li, Z. M.; Yan, F.; Dickson, B. M.; Guo, A. H.; Cantu, D. V.; Kaustov, L.; Brown, P. J.; Arrowsmith, C. H.; Erie, D. A.; Major, M. B.; Klevit, R. E.; Krajewski, K.; Kuhlman, B.; Strahl, B. D.; Rothbart, S. B. Hemi-Methylated DNA Regulates DNA Methylation Inheritance through Allosteric Activation of H3 Ubiquitylation by UHRF1. *Elife* **2016**, *5*, 1−24.
(23) Nady, N.; Lemak, A.; Walker, J. R.; Avvakumov, G. V.; Kareta, M. S.; Achour, M.; Xue, S.; Duan, S.; Allali-Hassani, A.; Zuo, X.; Wang, Y. X.; Bronner, C.; Chédin, F.; Arrowsmith, C. H.; Dhe-Paganon, S. Recognition of Multivalent Histone States Associated with Heterochromatin by UHRF1 Protein. *J. Biol. Chem.* **2011**, *286*, 24300−24311.
(24) Rothbart, S. B.; Krajewski, K.; Nady, N.; Tempel, W.; Xue, S.; Badeaux, A. I.; Barsyte-Lovejoy, D.; Martinez, J. Y.; Bedford, M. T.; Fuchs, S. M.; Arrowsmith, C. H.; Strahl, B. D. Association of UHRF1 with Methylated H3K9 Directs the Maintenance of DNA Methylation. *Nat. Struct. Mol. Biol.* **2012**, *19*, 1155−1160.
(25) Kong, X.; Chen, J.; Xie, W.; Brown, S. M.; Cai, Y.; Wu, K.; Fan, D.; Nie, Y.; Yegnasubramanian, S.; Tiedemann, R. L.; Tao, Y.; Ray-Whay, C. Y.; Topper, M. J.; Zahnow, C. A.; Easwaran, H.; Rothbart, S. B.; Xia, L.; Baylin, S. B. Defining UHRF1 Domains That Support Maintenance of Human Colon Cancer DNA Methylation and Oncogenic Properties. *Cancer Cell* **2019**, *35*, 633.e7−648.e7.
(26) Vaughan, R. M.; Dickson, B. M.; Whelihan, M. F.; Johnstone, A. L.; Cornett, E. M.; Cheek, M. A.; Ausherman, C. A.; Cowles, M. W.; Sun, Z.-W.; Rothbart, S. B. Chromatin Structure and Its Chemical Modifications Regulate the Ubiquitin Ligase Substrate Selectivity of UHRF1. *Proc. Natl. Acad. Sci. U. S. A.* **2018**, *115*, 8775−8780.
(27) Wang, F.; Yang, Y.-Z.; Shi, C.-Z.; Zhang, P.; Moyer, M. P.; Zhang, H.-Z.; Zou, Y.; Qin, H.-L. UHRF1 Promotes Cell Growth and Metastasis Through Repression of P16ink4a in Colorectal Cancer. *Ann. Surg. Oncol.* **2012**, *19*, 2753−2762.
(28) Jin, W.; Chen, L.; Chen, Y.; Xu, S.; Di, G.; Yin, W.; Wu, J.; Shao, Z. UHRF1 Is Associated with Epigenetic Silencing of BRCA1 in Sporadic Breast Cancer. *Breast Cancer Res. Treat.* **2010**, *123*, 359−373.
(29) Unoki, M.; Kelly, J. D.; Neal, D. E.; Ponder, B. A. J.; Nakamura, Y.; Hamamoto, R. UHRF1 Is a Novel Molecular Marker for Diagnosis and the Prognosis of Bladder Cancer. *Br. J. Cancer* **2009**, *101*, 98−105.
(30) Mudbhary, R.; Hoshida, Y.; Chernyavskaya, Y.; Jacob, V.; Villanueva, A.; Fiel, M. I.; Chen, X.; Kojima, K.; Thung, S.; Bronson, R. T.; Lachenmayer, A.; Revill, K.; Alsinet, C.; Sachidanandam, R.; Desai, A.; Sen Banerjee, S.; Ukomadu, C.; Llovet, J. M.; Sadler, K. C. UHRF1 Overexpression Drives DNA Hypomethylation and Hepatocellular Carcinoma. *Cancer Cell* **2014**, *25*, 196−209.
(31) Daskalos, A.; Oleksiewicz, U.; Filia, A.; Nikolaidis, G.; Xinarianos, G.; Gosney, J. R.; Malliri, A.; Field, J. K.; Liloglou, T. UHRF1-Mediated Tumor Suppressor Gene Inactivation in Nonsmall Cell Lung Cancer. *Cancer* **2011**, *117*, 1027−1037.
(32) Bárcena-Varela, M.; Caruso, S.; Llerena, S.; Álvarez-Sola, G.; Uriarte, I.; Latasa, M. U.; Urtasun, R.; Rebouissou, S.; Alvarez, L.; Jimenez, M.; Santamaría, E.; Rodriguez-Ortigosa, C.; Mazza, G.; Rombouts, K.; San José-Eneriz, E.; Rabal, O.; Agirre, X.; Iraburu, M.; Santos-Laso, A.; Banales, J. M.; Zucman-Rossi, J.; Prósper, F.; Oyarzabal, J.; Berasain, C.; Ávila, M. A.; Fernández-Barrena, M. G. Dual Targeting of Histone Methyltransferase G9a and DNA-Methyltransferase 1 for the Treatment of Experimental Hepatocellular Carcinoma. *Hepatology* **2019**, *69*, 587−603.
(33) Kofunato, Y.; Kumamoto, K.; Saitou, K.; Hayase, S.; Okayama, H.; Miyamoto, K.; Sato, Y.; Katakura, K.; Nakamura, I.; Ohki, S.; Koyama, Y.; Unoki, M.; Takenoshita, S. UHRF1 Expression Is Upregulated and Associated with Cellular Proliferation in Colorectal Cancer. *Oncol. Rep.* **2012**, *28*, 1997−2002.

https://doi.org/10.1021/acs.biochem.1c00698
Biochemistry 2022, 61, 354−366

(34) Senisterra, G.; Zhu, H. Y.; Luo, X.; Zhang, H.; Xun, G.; Lu, C.; Xiao, W.; Hajian, T.; Loppnau, P.; Chau, I.; Li, F.; Allali-Hassani, A.; Atadja, P.; Oyang, C.; Li, E.; Brown, P. J.; Arrowsmith, C. H.; Zhao, K.; Yu, Z.; Vedadi, M. Discovery of Small-Molecule Antagonists of the H3K9me3 Binding to UHRF1 Tandem Tudor Domain. *SLAS Discovery* **2018**, *23*, 930−940.
(35) Houliston, R. S.; Lemak, A.; Iqbal, A.; Ivanochko, D.; Duan, S.; Kaustov, L.; Ong, M. S.; Fan, L.; Senisterra, G.; Brown, P. J.; Wang, Y.-X.; Arrowsmith, C. H. Conformational Dynamics of the TTD-PHD Histone Reader Module of the UHRF1 Epigenetic Regulator Reveals Multiple Histone-Binding States, Allosteric Regulation, and Druggability. *J. Biol. Chem.* **2017**, *292*, 20947−20959.
(36) Chang, L.; Campbell, J.; Raji, I. O.; Guduru, S. K. R.; Kandel, P.; Nguyen, M.; Liu, S.; Tran, K.; Venugopal, N. K.; Taylor, B. C.; Holt, M. V.; Young, N. L.; Samuel, E. L. G.; Jain, P.; Santini, C.; Sankaran, B.; Mackenzie, K. R.; Young, D. W. Discovery of Small Molecules Targeting the Tandem Tudor Domain of the Epigenetic Factor UHRF1 Using Fragment-based Ligand Discovery. *Sci. Rep.* **2021**, *11*, 1−17.
(37) Wagner, E. K.; Albaugh, B. N.; Denu, J. M. High-Throughput Strategy to Identify Inhibitors of Histone-Binding Domains. *Methods Enzymol.* **2012**, *512*, 161−185.
(38) Arita, K.; Isogai, S.; Oda, T.; Unoki, M.; Sugita, K.; Sekiyama, N.; Kuwata, K.; Hamamoto, R.; Tochio, H.; Sato, M.; Ariyoshi, M.; Shirakawa, M. Recognition of Modification Status on a Histone H3 Tail by Linked Histone Reader Modules of the Epigenetic Regulator UHRF1. *Proc. Natl. Acad. Sci. U. S. A.* **2012**, *109*, 12950−12955.
(39) Lu, R.; Wang, G. G. Tudor: A Versatile Family of Histone Methylation 'Readers'. *Trends Biochem. Sci.* **2013**, *38*, 546−555.
(40) Bannister, A. J.; Zegerman, P.; Partridge, J. F.; Miska, E. A.; Thomas, J. O.; Allshire, R. C.; Kouzarides, T. Selective Recognition of Methylated Lysine 9 on Histone H3 by the HP1 Chromo Domain. *Nature* **2001**, *410*, 120−124.
(41) Fang, J.; Cheng, J.; Wang, J.; Zhang, Q.; Liu, M.; Gong, R.; Wang, P.; Zhang, X.; Feng, Y.; Lan, W.; Gong, Z.; Tang, C.; Wong, J.; Yang, H.; Cao, C.; Xu, Y. Hemi-Methylated DNA Opens a Closed Conformation of UHRF1 to Facilitate Its Histone Recognition. *Nat. Commun.* **2016**, *7*, 1−12.
(42) Gelato, K. A.; Tauber, M.; Ong, M. S.; Winter, S.; Hiragami-Hamada, K.; Sindlinger, J.; Lemak, A.; Bultsma, Y.; Houliston, S.; Schwarzer, D.; Divecha, N.; Arrowsmith, C. H.; Fischle, W. Accessibility of Different Histone H3-Binding Domains of UHRF1 Is Allosterically Regulated by Phosphatidylinositol 5-Phosphate. *Mol. Cell* **2014**, *54*, 905−919.
(43) Lallous, N.; Legrand, P.; McEwen, A. G.; Ramón-Maiques, S.; Samana, J.-P.; Birck, C. The PHD Finger of Human UHRF1 Reveals a New Subgroup of Unmethylated Histone H3 Tail Readers. *PLoS One* **2011**, *6*, 1−11.
(44) Hu, L.; Li, Z.; Wang, P.; Lin, Y.; Xu, Y. Crystal Structure of PHD Domain of UHRF1 and Insights into Recognition of Unmodified Histone H3 Arginine Residue 2. *Cell Res.* **2011**, *21*, 1374−1378.
(45) Sanchez, R.; Zhou, M. The PHD Finger: A Versatile Epigenome Reader. *Trends Biochem. Sci.* **2011**, *36*, 364−372.
(46) Org, T.; Chignola, F.; Hetényi, C.; Gaetani, M.; Rebane, A.; Liiv, I.; Maran, U.; Mollica, L.; Bottomley, M. J.; Musco, G.; Peterson, P. The Autoimmune Regulator PHD Finger Binds to Non-Methylated Histone H3K4 to Activate Gene Expression. *EMBO Rep.* **2008**, *9*, 370−376.
(47) Lan, F.; Collins, R. E.; De Cegli, R.; Alpatov, R.; Horton, J. R.; Shi, X.; Gozani, O.; Cheng, X.; Shi, Y. Recognition of Unmethylated Histone H3 Lysine 4 Links BHC80 to LSD1-Mediated Gene Repression. *Nature* **2007**, *448*, 718−722.
(48) Wang, G. G.; Song, J.; Wang, Z.; Dormann, H. L.; Casadio, F.; Li, H.; Luo, J. L.; Patel, D. J.; Allis, C. D. Haematopoietic Malignancies Caused by Dysregulation of a Chromatin-Binding PHD Finger. *Nature* **2009**, *459*, 847−851.
(49) Matthews, A. G. W.; Kuo, A. J.; Ramón-Maiques, S.; Han, S.; Champagne, K. S.; Ivanov, D.; Gallardo, M.; Carney, D.; Cheung, P.; Ciccone, D. N.; Walter, K. L.; Utz, P. J.; Shi, Y.; Kutateladze, T. G.; Yang, W.; Gozani, O.; Oettinger, M. A. RAG2 PHD Finger Couples Histone H3 Lysine 4 Trimethylation with V (D) J Recombination. *Nature* **2007**, *450*, 1106−1111.
(50) Wang, C.; Shen, J.; Yang, Z.; Chen, P.; Zhao, B.; Hu, W.; Lan, W.; Tong, X.; Wu, H.; Li, G.; Cao, C. Structural Basis for Site-Specific Reading of Unmodified R2 of Histone H3 Tail by UHRF1 PHD Finger. *Cell Res.* **2011**, *21*, 1379−1382.
(51) Cheng, J.; Yang, Y.; Fang, J.; Xiao, J.; Zhu, T.; Chen, F.; Wang, P.; Li, Z.; Yang, H.; Xu, Y. Structural Insight into Coordinated Recognition of Trimethylated Histone H3 Lysine 9 (H3K9me3) by the Plant Homeodomain (PHD) and Tandem Tudor Domain (TTD) of UHRF1 (Ubiquitin-like, Containing PHD and RING Finger Domains, 1) Protein. *J. Biol. Chem.* **2013**, *288*, 1329−1339.
(52) Machleidt, T.; Woodroofe, C. C.; Schwinn, M. K.; Méndez, J.; Robers, M. B.; Zimmerman, K.; Otto, P.; Daniels, D. L.; Kirkland, T. A.; Wood, K. V. Nano BRET−A Novel BRET Platform for the Analysis of Protein-Protein Interactions. *ACS Chem. Biol.* **2015**, *10*, 1797−1804.
(53) Wan, X.; Yang, S.; Huang, W.; Wu, D.; Chen, H.; Wu, M.; Li, J.; Li, T.; Li, Y. UHRF1 Overexpression Is Involved in Cell Proliferation and Biochemical Recurrence in Prostate Cancer after Radical Prostatectomy. *J. Exp. Clin. Cancer Res.* **2016**, *35*, 1−14.
(54) Babbio, F.; Pistore, C.; Curti, L.; Castiglioni, I.; Kunderfranco, P.; Brino, L.; Oudet, P.; Seiler, R.; Thalman, G. N.; Roggero, E.; Sarti, M.; Pinton, S.; Mello-Grand, M.; Chiorino, G.; Catapano, C. V.; Carbone, G. M.; Bonapace, I. M. The SRA Protein UHRF1 Promotes Epigenetic Crosstalks and Is Involved in Prostate Cancer Progression. *Oncogene* **2012**, *31*, 4878−4887.
(55) Crouch, S. P. M.; Kozlowski, R.; Slater, K. J.; Fletcher, J. The Use of ATP Bioluminescence as a Measure of Cell Proliferation and Cytotoxicity. *J. Immunol. Methods* **1993**, *160*, 81−88.
(56) Rothbart, S. B.; Dickson, B. M.; Ong, M. S.; Krajewski, K.; Houliston, S.; Kireev, D. B.; Arrowsmith, C. H.; Strahl, B. D. Multivalent Histone Engagement by the Linked Tandem Tudor and PHD Domains of UHRF1 Is Required for the Epigenetic Inheritance of DNA Methylation. *Genes Dev.* **2013**, *27*, 1288−1298.
(57) Vaughan, R. M.; Kupai, A.; Foley, C. A.; Sagum, C. A.; Tibben, B. M.; Eden, H. E.; Tiedemann, R. L.; Berryhill, C. A.; Patel, V.; Shaw, K. M.; Krajewski, K.; Strahl, B. D.; Bedford, M. T.; Frye, S. V.; Dickson, B. M.; Rothbart, S. B. The Histone and Non-histone Methyllysine Reader Activities of the UHRF1 Tandem Tudor Domain Are Dispensable for the Propagation of Aberrant DNA Methylation Patterning in Cancer Cells. *Epigenet. Chromatin* **2020**, *13*, 1−15.
(58) Wagner, E. K.; Nath, N.; Flemming, R.; Feltenberger, J. B.; Denu, J. M. Identification and Characterization of Small Molecule Inhibitors of a Plant Homeodomain Finger. *Biochemistry* **2012**, *51*, 8293−8306.
(59) Amato, A.; Lucas, X.; Bortoluzzi, A.; Wright, D.; Ciulli, A. Targeting Ligandable Pockets on Plant Homeodomain (PHD) Zinc Finger Domains by a Fragment-Based Approach. *ACS Chem. Biol.* **2018**, *13*, 915−921.
(60) Miller, T. C. R.; Rutherford, T. J.; Birchall, K.; Chugh, J.; Fiedler, M.; Bienz, M. Competitive Binding of a Benzimidazole to the Histone-Binding Pocket of the Pygo PHD Finger. *ACS Chem. Biol.* **2014**, *9*, 2864−2874.

https://doi.org/10.1021/acs.biochem.1c00698
Biochemistry 2022, 61, 354−366